Journal of Materials Chemistry C

Accepted Manuscript

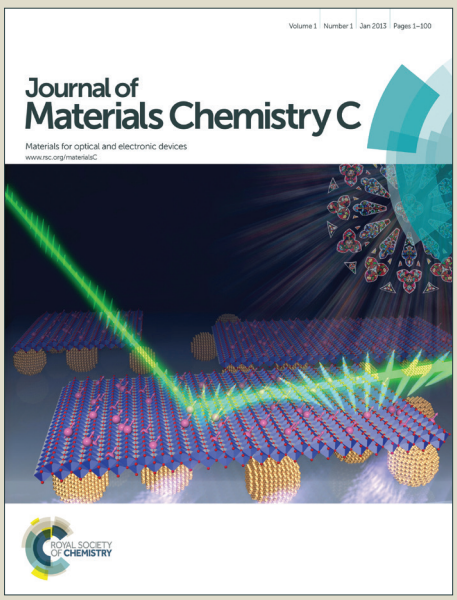

ROYAL SOCIETY OF CHEMISTRY

www.rsc.org/materialsC

Lumino-Magnetic YAG:Ce Nanophosphors: Novel Synthesis Routes For Efficient Luminescence And Magnetic Properties

K.Jayanthi* and Sunkara V Manorama*

Nanomaterials Laboratory, Inorganic and Physical Chemistry Division, CSIR-Indian Institute of Chemical Technology, Hyderabad -500007, India.

ABSTRACT

Recent efforts in developing spintronic and magneto-optoelectric materials for applications have relied on the use of magnetic semiconductors doped with transition metals, but these have met with limited success. Remarkable ferromagnetism from luminescent insulators with Curie temperature above room temperature (>600K) is an exceptional class of materials for magneto-optoelectronic and biological applications. A facile and elegant synthesis methodology is one of the key factors to achieve efficient luminescent and magnetic properties in nanoscale materials. Different strategies adopted to prepare Ce doped YAG nanophosphors have been described and their structural, luminescent and magnetic properties studied. It is anticipated that lattice defects (vacancies) present in the complex yttrium aluminium oxide lattice are responsible for the observed ferromagnetism and an explicit correlation emerges between defects/vacancies present in the YAG lattice with the luminescent and magnetic properties. The luminescence decreased at low synthesis temperature conditions and magnetization increased due to high

defects/vacancies and vice versa at high temperature. Interestingly the coercive field is observed to increase with increase in temperature and the possible mechanisms for these observations discussed.

Keywords: Lumino-magnetic Nanophosphors, YAG:Ce, ferromagnetism, Defects/vacancies, magneto-optoelectric devices

---

***Corresponding authors:**k.jayanthirajan@gmail.com; manorama@iict.res.in

▪ *INTRODUCTION*

Multifunctional luminescent - magnetic Nano-Phosphors (NPs) have emerged as a class of important futuristic materials for a variety of applications starting from Spin-Light Emitting Devices (Spin-LEDs), data storage, security devices and sensors to biomedical applications[1-4]. In nature, materials that exhibit significant magnetism at and above Room Temperature (RT) along with efficient luminescence behavior are very rare[5]. In semiconductors, transition metal doped luminescent ZnO is reported to exhibit ferromagnetism at RT and above, while existence of this ferromagnetism is still controversial and theoretically predicted to be very unstable[6,7]. In our earlier work we have reported that carrier induced high temperature ferromagnetism is possible from alkali metals (Li/Na) ZnO NPs even in the absence of any magnetic elements[8]. On the other hand, band insulators like HfO_2, $Ca_{1-x}La_xB_6$ are reported to show very strong ferromagnetism at and above RT,[9,10] for example thin films

of the band insulator HfO_2 have been reported to show strong FM up to temperatures >500K but these materials are not reported be luminescent materials.

Garnet structured Yttrium Aluminium Oxide (Y_2O_3-Al_2O_3) with cubic (YAG) and its tetragonal modifications (YAT); perovskite (YAP) and Monoclinic (YAM) modifications are well known luminescent materials in different wavelength regions depending on the dopant used. Particularly trivalent Cerium (Ce) doped YAG is yellow emitting phosphor materials which produces white light when used with a blue-LED[11,12]. Recently, we reported ferromagnetism from undoped and Ce doped YAG:Ce, YAT:Ce and YAM:Ce prepared by post heat solidified combustion technique[13]. The present study details the three major synthesis techniques which were adopted to optimize the luminescent and magnetic behavior of YAG:Ce NPs. From these studies it could be established that the synthesis conditions play a major role in influencing the luminescent and magnetic properties.

▪ *EXPERIMENTAL SECTION*

(i) ***Post Heat Solidified Combustion Technique (PHSCT):*** $Y_{3-x}Ce_xAl_5O_{12}$ [$Y_{2.7}Ce_{0.3}Al_5O_{12}$] NPs powders were successfully prepared by PHSCT under mild conditions using inexpensive aluminum and yttrium nitrates as the starting materials and urea as the homogenizing precipitant. The yttrium nitrate solution was obtained by dissolving Y_2O_3 in diluted nitric acid and 5ml of deionized water and the reaction continued by heating at 80^oC for 30 mins to get a clear solution, followed by evaporation of the excess acid. Aluminum nitrate and cerium nitrate were added to the above solution and then 0.1M of urea was added till a clear solution was obtained and this was kept in a preheated

furnace (550^{o}C) for 20 mins to obtain a fluffy mass. The material obtained was ground and subsequently fired at 1300^{o}C for 4 hrs in air atmosphere to obtain the product.

(ii) ***Post Heated Hydrothermal-Homogenous Precipitation Technique (PHHHPT):*** Clear precursor solution (Same as PHSCT) was prepared and transferred to a hydrothermal container in a preheated oven and maintained at 180^{o}C for 24 hrs. The clear liquid was decanted and the YAG:Ce powder settled at the bottom was repeatedly washed with ethanol ultrasonically. The washing was necessary to get rid of the surface impurities and minimize the particle agglomeration. Prepared YAG:Ce powder was dried in an oven and subsequently fired at 1300^{o}C for 4 hrs in air atmosphere. Any possibility of magnetic contamination accidentally or inclusion of trace impurities has been meticulously avoided by taking utmost care while choosing the precursors and special care was taken during the synthesis procedure. Fresh high-purity glass ware without any metallic contamination was used throughout.

(iii) ***Post Heated Auto-Clave Technique (PHACT):*** Clear precursor solution (Same as in PHSCT) about 10ml was taken, made up to 70 ml using DI water and placed in a high pressure (30 Torr) auto-clave with continuous stirring at 180^{o}C for 2.5 hrs. The prepared YAG:Ce powder was washed with ethanol and dried in an oven and subsequently fired at 1300^{o}C for 4 hrs in air atmosphere.

▪ CHARACTERIZATION

(i) Structure and morphology studies: The synthesized materials were characterized for their structure and morphology by powder X-Ray Diffraction (XRD) on a Siemens D5000 (Cheshire, UK)

instrument over a 2Θ range of 2° to 60° using CuKα radiation (λ=1.5406Å) at 40 kV and 30mA with a standard monochromator using Ni filter and the TEM on a Philips Technai G2 FEI F12 system operating at 80–120 kV). The average crystallite size of the samples was estimated by applying the Scherrer equation to the major diffraction peaks. For Transmission Electron Microscopy studies (TEM, Philips Technai G2 FEI F12), the samples were dispersed in ethanol by ultra-sonication and then loaded on to formvar-coated copper grids. The grids were air-dried before recording the micrographs. The morphology of the products was observed on a Scanning Electron Microscopy (SEM) HITACHI S-3400N system.

(ii) ***^{27}Al solid state MAS-NMR study:*** Solid state Magic Angle Spinning - Nuclear Magnetic Resonance (MAS-NMR) is used as an effective tool to establish the chemical composition especially to distinguish the different structures with similar chemical entities. MAS-NMR is very important where there is short range order and is a complementary tool to XRD which is effective when there is long range order. The MAS-NMR measurements were performed on a Bruker ultra shield 500MHz WB NMR spectrometer in an 11.75 T field producing ^{27}Al Larmor frequency at 130.31 MHz. The samples were placed in a 3.2 mm rotor and the spinning rate was set at 10 kHz. The applied pulse width corresponding to an angle of $\pi/2$ for ^{27}Al is 4 μs with a pulse delay of 10s and the pulse sequence applied is the normal single pulse. The chemical shift reference was set at 0 ppm corresponding to the Aluminium Nitrate single peak.

(iii) ***X-Ray Photo Electron Spectroscopy (XPS):*** XPS spectra were obtained using SPECS XPS system (M/s.SPECS Surface Nano Analysis GmbH, Germany) equipped with twin anode X-ray

source and a hemispherical analyzer with a single-channel detector. The spectra were obtained with 150W non-monochromatic Al Kα radiation (1486.6 eV).

(iv) Photoluminescence studies (PL): The RT PL spectrum was recorded in double monochromator based Cary Eclipse luminescence spectrometer (AGILENT Technologies) with xenon flash lamp as a source of excitation.

(v) Magnetic studies: Magnetization (*M-H)* of the YAG:Ce NPs powder samples was measured at RT using a Micro-sense Vibrating Sample Magnetometer (VSM) using a glass rod wrapped with aluminium foil as the sample holder. Variation in magnetization and coercive field with temperature was recorded using VSM for Curie temperature determination. The results of magnetic measurements were reproducible for all the samples.

(vi) ZFC-FC studies: Low temperature (less then 130K) magnetic measurements were performed using a Superconducting Quantum Interference Device (SQUID) magnetometer MPMS-5P, operating between 5 to 300K for dc-applied fields ranging from −5 to 5 T. Zero-field cool/field cool and hysteresis measurements were performed on centrifuged and dried nanophosphor samples that were all wrapped in polyethylene membrane. The Zero-Field Cooled/Field Cooled (ZFC/FC) measurements were taken between 5 to 300K, with an applied field of 100 Oe, and the hysteresis measurements were performed at RT.

(vii) Atomic Force and Magnetic Force Microscopy (AFM-MFM) measurements: To confirm the RT ferromagnetism of the samples, as well as to study their magnetic domain structure, MFM

measurements were performed at RT. The surface topography and magnetic phase shift profiles of the NPs were mapped by using MFM module in scanning probe microscopy from NT-MDT (Russia, Model-Aura), in semi-contact mode. Silicon cantilevers (NSG-01/Co, from NT-MDT) coated with cobalt/chromium film having coating thickness 30-40 nm, tip radius ~40 nm, and resonance frequency 222 kHz, were used. All the results reported in the present work were carried out under the external magnetic field of 1000 Gauss. The samples for the measurements were prepared by compacting the nanophosphor particulate powder. Throughout this work, a nonmagnetic SMENA head (the AFM head was used, which acts as a probe holder as well as scanner) and sample holder that were made up of nonmagnetic materials to minimize the errors in the measurements.

(ix) Electron Paramagnetic Resonance (EPR) Studies: The EPR spectra were acquired with a JEOL (JES-FA 200) X-band spectrometer operating at 9.45 GHz (Microwave Frequency) and 100 kHz (Modulation Frequency) at room temperature.

▪ RESULTS AND DISCUSSION

Structural Studies of YAG:Ce NPs. The YAG phase formation under various synthesis conditions was studied by XRD and the results are found to be in good agreement with reported data (JCPDS Card No:33-0040), establishing that each final product consists of the single phase of corresponding crystalline YAG nanocrystalline structure without presence of any byproduct phase (YAP, YAM) as shown in Figure 1. Prior to annealing, the NPs prepared by all the techniques are found to be amorphous [Supplementary Information (SI) Figure 1]. However on heating to 1300^{o}C, highly crystalline NPs with YAG structure are formed. From the line width of the XRD peaks, the

average crystallite size D is calculated using the Scherrer equation $D = K\lambda/\beta Cos\theta$, where K is the shape factor, λ the wavelength of the X-rays used, β is the FWHM of the peak and θ is the Bragg angle. The crystallite size is found to be ~20-25 nm. 0.1M% Ce doped YAG NPs prepared by PHSC technique does not show any phase related to dopant atoms, however samples prepared by PHHHPT and PHACT at similar mole percentage shows precipitated secondary phase of Ce_2O_3 (marked as * in XRD) confirming that the dopant has reached optimum incorporation in the host lattice. To confirm the solubility limit of dopant in PHSC technique, experiments with different Ce concentration were carried out and the results are shown in SI Figure 2. Secondary precipitated phase of Ce_2O_3 are visible from 0.2M% of Ce doped YAG NPs that increases with increase in Ce concentration (0.5M%). The results indicate that synthesis conditions are playing a major role in incorporation of activator in to the host lattice. The lattice parameters were calculated from the XRD peaks and found to be 12.0613 Å for NPs prepared by PHSCT and 12.0511 and 12.0498 Å for PHHHPT and PHAC techniques. To confirm the effect of dopant at high Ce concentration we calculated lattice parameters of undoped and different Ce concentration doped YAG NPs prepared by PHSC technique and the results are tabulated in Table 1. Lattice parameters increased with increasing Ce concentration up to 0.1M% and were stable with increase in Ce concentration (0.2M%) and decreased with further increase in Ce to 0.5M%. The increase in lattice parameter for the Ce doped samples prepared by all the techniques compared to the undoped one has been attributed to higher ionic radii of Ce^{3+} (1.15A˚) compared toY^{3+} ions (1.04A˚)[14]. Lattice parameters increased with increasing Ce concentration up to 0.1M% and were stable with increase in Ce concentration (0.2M%). With further increase in Ce to 0.5M%, a decrease in the cell parameters was observed. The increase in lattice parameter for the Ce doped samples compared to the undoped can been attributed to higher ionic radii of Ce^{3+} (1.15A˚) compared to the Y^{3+} ions (1.04A˚).

On the other hand above 0.2M% which is the solubility limit of Ce in the YAG lattice, some of the incorporated Ce ions could possibly convert into Ce^{4+} with a smaller ionic radius and this could be responsible for the observed decreased cell parameters. This type of conversion from Ce^{3+} to Ce^{4+} is possible under the conditions of calcinations which were carried out in air atmosphere. There are several earlier reports on similar such observations[15, 16]. Furthermore, the lattice parameters of 0.1M% Ce doped YAG NPs prepared by PHSC technique is found to be higher than that of other two techniques indicating that there is maximum incorporation of Ce in Y site in this sample. In YAG lattice, Y^{3+} ions are having an eight coordinated dodecahedral symmetry[17] and Ce^{3+} ions when incorporated in the lattice occupy the Y^{3+} sites due to similar radii compared with smaller radii of Al^{3+} (0.67Å). In addition, the patterns of YAG:Ce NPs prepared by PHSCT showed clear shifts to lower 2θ angles up 0.2M% (SI Table 1) compared to undoped NPs prepared by same technique, attributed to the dopant incorporation and nanosize effect[18,19] and further shift to lower angle at 0.5M% Ce ascertained that the dopant reached an optimum solubility limit at 0.2M%.

Morphology studies. Drastic change in morphology has been observed in YAG:Ce NPs depending upon the synthesis conditions as shown in the TEM images [Figure 2a, b, c]. Uniform nanowire formation with width of about 5 nm and length varying from 20 to 200 nm has been observed in samples prepared by PHHHP technique and spherical formation with size of about 20 to 30 nm has been observed in samples prepared by PHAC technique, where as honeycomb like agglomerated spherical structure formation few hundred nanometer in size with individual particle size of about 10-15 nm with PHSC technique. SEM images of NPs samples prepared by combustion technique further reconfirmed the honeycomb formation (Figure 2d). Results clearly indicate that the same precursor solutions under different synthesis conditions and temperature could affect the size

and morphology of the YAG:Ce NPs. Such variation in the morphology due to temperature and dopant effect has been reported in our earlier work on ZnO NPs[20]. Spherical morphology is an important factor for reducing the amount of light scattering at the surfaces and increasing the packing density[21-23] and for this reason the materials obtained by PHACT and PHSC techniques would be ideally suited for better device performance.

Photoluminescence studies. PL excitation and emission spectra of Ce doped YAG NPs prepared at different conditions are depicted in Figure 3a. Figure 3b shows the variation of luminescence efficiency with Ce concentration (0.05M% to 0.5M%). PL intensity increased up to 0.1M% of Ce and maintained almost same intensity at 0.2M% and decreased from 0.3M% of Ce doped YAG. Hence, 0.1M% was chosen as an optimum concentration and further experiments were performed with this Ce molar ratio.

The emission spectra of YAG:Ce NPs prepared under various synthesis conditions show characteristic emission of Ce^{3+} at 555 nm that corresponds to the 4f to 5d transition level of Ce^{3+} [24,25] which is excitable by 460 nm (inset of Figure 3a). YAG:Ce NPs prepared by PHSC techniques show maximum emission intensity compared with other two techniques taken at identical conditions. Results are in good agreement with XRD results that indicate that the NPs prepared by PHSCT show maximum incorporation of Ce (no precipitated phase of Ce observed at 0.1M% Ce) compared to other two techniques which shows precipitated secondary phase of Ce at 0.1M% leading to high efficiency in PL results. Besides the absence of longer wavelength emission (~780-800 nm) which is associated with iron impurities[26,27] this observation also confirms the purity of YAG:Ce NPs.

To establish the emission properties of pure YAG, undoped YAG NPs were synthesized by all three methods while maintaining all experimental conditions similar to the doped samples. An interesting observation is that the undoped YAG NPs prepared by PHACT technique exhibits maximum luminescence efficiency followed by PHHHPT compared with samples prepared by PHSC technique which shows maximum efficiency related to Ce emission [SI Figure 3]. Compared to Ce doped NPs, undoped samples exhibit lower efficiency as shown in SI Figure 3. Intrinsic defects, predominantly oxygen vacancy (V_O) could be responsible for observed high efficiency from NPs prepared by PHACT technique at low temperature (180^{o}C for PHACT and PHHHP techniques compared with 550^{o}C for PHSC technique) as the most convenient to form and more stable than other charged species at low temperature[28] which has been observed from XPS and EDS analysis. Observed low efficiency from pure YAG NPs compared with Ce doped YAG is well known and trap levels related to Vo act as luminescence quenchers[29] because the excited electrons would recombine or get trapped at the nearest defective sites and cause the non-radiative relaxation.

NMR and XPS studies. The sensitivity of MAS ^{27}Al NMR chemical shifts towards the co-ordination state of Al^{III} is increasingly being used for identifying the different phases and co-ordination states of Al centers and phases related to impurity atoms in aluminum containing materials[30,31]. The ^{27}Al MAS NMR spectra of the YAG:NPs prepared by PHSC technique is shown in Figure 4a. According to several studies[31,32], the solid state structure of $Y_3Al_5O_{12}$ consists of a network of four, five and six- fold co-ordinated aluminum atoms. Chemical shifts of different coordination states of Al atoms are well recognizable: octahedral AlO_6 sites resonate between 15 −30 ppm, the much less common AlO_5 sites between 40 - 25 ppm and tetrahedral AlO_4 between 80 -50 ppm. On this account, the 9.916 ppm major resonance in the spectrum corresponds to six-coordinate

aluminum$^{(III)}$. Besides, other distinct broad peaks located at about 39.645 ppm and 87.896, 67.398 ppm can be assigned to five and four-fold coordinated aluminum atoms. It can be noticed that the resonance at 39.645 ppm can also be consistent with a tetrahedral site distorted due to the presence of oxygen defects[31, 33-35]. Mackenzie et *al*[33], suggested that the AlO_5 site could give rise to transient hexagonal $YAlO_3$. In our sample, this process does not occur, as shown in XRD spectra where no diffraction peak associated with the perovskite structure was observed (Figure 1) leading to conclude that presence of oxygen defects are responsible for this phase. As for the chemical valence state of Ce ions in Ce-doped YAG NPs, an XPS analysis was carried out and results are shown in Fig. 4b. It can be noted that the XPS of the Ce-doped sample gives two distinct characteristic peaks at the binding energies of 886 and 903eV, which exactly correspond to the $Ce^{3+}3d_{5/2}$ and $Ce^{3+}3d_{3/2}$, respectively due to the 3d orbital split of Ce^{3+} ions[36] by the spin-orbit coupling effect. Therefore, it can be concluded that the Ce ions in Ce-doped YAG NPs exists in a single chemical valence of +3.

Magnetic studies. Magnetic properties of the undoped and Ce doped YAG NPs were determined from VSM and SQUID magnetometry analysis. Magnetization measurements carried out at RT for undoped and Ce doped (0.1M%) YAG NPs prepared by above mentioned synthesis routes shows typical hysteresis loops as shown in Figure 5 (a, b). Compared to doped NPs, undoped YAG synthesized in exactly identical experimental conditions show slightly high magnetization (M) and coercive field (H_C) as shown in Table 2. Maximum M value observed was 78.14 memu/g with H_C of 17.29 Oe with NPs prepared by PHAC technique. Similarly, high H_C obtained with NPs prepared with PHSCT (54.50 Oe) with magnetization value of 31.83 memu/g as shown in inset of Figure 5a. RT M-H value of YAG:Ce NPs prepared by PHSC technique by changing the dopant concentration show similar values[13] and H_C continuously increased with decrease in temperature (200, 130K) and

vice versa above RT (400, 500 and 600K) while maintaining M nearly constant. The H_C of 42.12 Oe and M of 8.93 memu/g at 600K shows that Curie temperature (T_C) will be higher than 600K as we could not probe further due to instrumental limitation. In order to exclude any origin other than intrinsic to the observed magnetic behavior of YAG samples, sample synthesis, handling process, and measurements were done with utmost care. Since extreme precautions were taken to avoid any magnetic contamination during different steps involved in experimental process, the only probable suspect could be trace magnetic impurities present in the precursor materials. Hence highly pure Yttrium (III) Oxide (Y_2O_3, 99.99% pure) and Aluminium Nitrate Nonahydrate ($Al(NO_3)_3$ $9H_2O$, 99.997% pure) were used as a precursors and the observed high stable ferromagnetism and T_C, stable at 130 and 600 K cannot be attributed to any trace impurities. XRD, EDS, PL and XPS analysis also clearly reveals the absence of any magnetic elements. Another justification to support our claim for the absence of any magnetic impurity is that, in case magnetic impurities are present their effect would be consistent throughout the temperature range but as observed the coercive field has a characteristic temperature response.

Formation of magnetic domains is basic to the origin of ferromagnetism, hence the topography and magnetic phase mapping of YAG;Ce magnetic structure was investigated by high resolution AFM and MFM on pellets of NPs. The contrast/brightness profile in magnetic phase map and topography clearly shows the internal nature of the ferromagnetism and magnetic domains with a near uniform distribution at RT.

For a further insight into the magnetic properties of YAlO NPs at low temperatures (less than 130K), The magnetization versus temperature properties were studied using Quantum Design's SQUID magnetometer equipped with a 5-T magnet in the temperature range of 5 to 300 K. Figure 6 shows

the magnetization of undoped and 0.1M Ce doped YAG NPs prepared by PHSC technique as a function of temperature obtained at the ZFC and FC conditions with an applied magnetic field of 100 Oe. Superimposition of ZFC/FC plots[35] between 150 to 300 K as well as clear separation between the FC and ZFC processes at low temperature without blocking temperature[38-41] indicate that YAG:Ce NPs are ferromagnetic in nature. Measuring ZFC/FC curves is also an effective method for determining the presence of any magnetic impurities[42]. Magnetic impurities, if present show up as a blocking temperature that can be observed in the ZFC/FC curves. No signal for blocking temperature was observed in the ZFC curves, which implies that no magnetic nanoparticles exist in all the samples within the measured temperature range. In addition, presence of magnetic hysteresis loops with saturation magnetization and coercive field values of approximately 1.19 memu/g and 168.50 Oe observed at RT SQUID measurements taken for Ce doped YAG (inset of Fig 6) further supports our claim.

To further confirm the existence of oxygen vacancies, EPR spectra of the undoped and 0.1M% Ce doped YAG NPs has been carried out and results are shown in Fig. 7. It is observed that all samples exhibit the broad strong symmetric EPR peak with g = 2.06 (Undoped YAG) and 2.14 (YAG:Ce) with sharp peaks appeared at g value of 3.01 for both the NPs. A broad signal that appears at the lower field is attributed to ferromagnetic-resonance which arises from transition within the ground state of the ferromagnetic domain[43,44], and a narrow ESR signal arising from the paramagnetic states of surface defects[45,46]. However, it is believed that this narrow signal is not involved in the ferromagnetic ordering[47,48]. The EPR signal with g=2.00 to 2.15 was reported and referred to as due to oxygen vacancy[46, 47, 49.] Similar values are reported for TiO_2 and ZnO and reported to be due to oxygen vacancies Vo[46,50].

As yttrium and aluminium are non-magnetic elements, the origin of ferromagnetism of these nonmagnetic oxides could be attributed solely to the defects and/or oxygen vacancies similar to that in the thin films of HfO_2[9], TiO_2[51], CaB_6[52], CaO[53], SiC[54] and In_2O_3[51]. We strongly believe that unpaired spins have their origin in the oxygen vacancies that could be responsible for the observed magnetic moment of undoped and Ce doped YAG NPs as evidenced from PL and XPS analysis which shows presence of V_O. The strong evidence of magnetic properties due to V_O comes from PL studies of undoped YAG NPs prepared by PHACT that show maximum emission which could have been caused by oxygen defects giving maximum magnetization and this decreased with increase in temperature and supported by EPR analysis of these samples which shows strong symmetrical signal at g=2.06 and 2.14 suggesting some sort of exchange interactions among the localized electron spin moments from single electron trapped in oxygen vacancies (*F* center) are polarized to give room-temperature ferromagnetism as suggested by M. Venkatesan[9] and S. Tsunekawa et al[55].

▪ CONCLUSIONS

The present study established that yellow emitting YAG:Ce NPs exhibits stable ferromagnetism up to and above 600K. The discovery of ferromagnetism from undoped and doped insulator materials like YAG:Ce NPs prepared by different synthesis routes has directed our attention to a new, nevertheless not so uncommon phenomena of d^o magnetism, or magnetism due to defects and/or oxygen vacancies that has been experimentally validated by magnetic hysteresis loop, ZFC-FC studies and EPR analysis. Such novel ferromagnetic phenomena based on multifunctional materials such as YAG:Ce could pave the way for a new class of magnetooptic and spintronic materials for a wide variety of applications.

▪ ACKNOWLEDGEMENTS

K. Jayanthi acknowledges CSIR-Nehru Science Postdoctoral Research Fellowship Scheme (HRDG/CSIR-Nehru PDF/EN-ES-PS/EMR-1/02/2012) for the financial support and the authors duly acknowledge the strong support of the CSIR XII-FYP Projects M2D (CSC-0134) and IntelCOAT (CSC-0114) for the grants received.

▪ REFERENCES

1. Rémi Beaulac, Lars Schneider, Paul I. Archer, Gerd Bacher, Daniel R. Gamelin, *Science.,* 2009, **325**, 973-976.
2. Ce´line Hoffmann, Elsa Mazari, Sylvie Lallet, Roland Le Borgne, Vale´rie Marchi, Charlie Gosse, Zoher Gueroui, *Nature Nanotechnology.,* 2013, **8***,* 199-205.
3. Bipin Kumar Gupta, D Haranath, Shikha Saini, V N Singh, V Shanker, *Nanotechnology.,* 2010, **21***,* 055607.
4. Tharangattu N. Narayanan, Bipin K. Gupta, Sajna A, Vithayathil, Rebeca R. Aburto, Sendurai A. Mani, Jaime Taha-Tijerina, Bin Xie, Benny A. Kaipparettu, Suzy V. Torti, and Pulickel M. Ajayan, *Adv. Mater.,* 2012, **24**, 2992–2998.
5. Bipin Kumar Gupta, Vimal Rathee , Tharangattu N. Narayanan, Palanisamy Thanikaivelan, Avishek Saha, Govind, S. P. Singh, V. Shanker, Angel A. Marti, and Pulickel M. Ajayan., *Small.,* 2011, **7,** 1767–1773.

6. Ram Seshadri, *Curr. Opin*. *Solid State Mater. Sci.*, 2005, **9**, 1.

7. Sundaresan A, Bhargavi R, Rangarajan N, Siddesh U, and C. N. R. Rao, Phys. *Re B.,* 2006, **74,** 161306

8. Santa Chawla, K. Jayanthi, and R. K. Kotnala, *Phys. Rev B.,* 2009, **79**, 125204.

9. M. Venkatesan, C. B. Fitzgerald, J.M.D. Coey, *Nature.,* 2004**,** 430, 630.

10. D. P. Young, D. Hall, M. E. Torelli, Z. Fisk, J. D. Thomson, H. R. Ott, S. B. Oseroff, R. G. Goodrich, and R. Zysler, *Nature.,* 1999, 397, 412.

11. Biao Dong, Jing Wang, Jiao Sun, Sai Xu, Xue Bai, Zhenlong Jiang, Lei Xia, Liankun Sun, and Hongwei Song, *RSC Advances.,* 2012, **2**, 3897–3905.

12. Abdelhay Aboulaich, Martyna Michalska, Raphaël Schneider, Audrey Potdevin, Jérôme Deschamps, Rodolphe Deloncle, Geneviève Chadeyron, and Rachid Mahiou, *ACS Appl. Mater. Interfaces.,* 2014**, 6**, 252−258.

13. K. Jayanthi, M. Mohan Rao, L. Satyanarayana, M. Manivel Raja, Kuntumalla Mohan Kumar, Vadali V.S.S.Srikanth, Munisamy Subrahmanyam, C. Anandan, and Sunkara V Manorama, *ACS Nano.*, 2014, Submitted.

14. Alexander Birkel, Kristin A. Denault, Nathan C. George, Courtney E. Doll, Bathylle Héry, Alexander A. Mikhailovsky, Christina S. Birkel, Byung-Chul Hong, and Ram Seshadri, *Chem. Mater.,* 2012, **24**, 1198−1204.

15. Hsuan-Min Lee, Chao-Chi Cheng, Chi-Yuen Huang, Materials Research Bulletin., 2009, **44,** 1081-1085.

16. Maria Luisa Saladino, Eugenio Caponetti, Delia Chillura Martino, Stefano Enzo, Giulio Ibba, *Optical Materials*., 2008, **31**, 261–267.

17. S. Mukherjee, V. Sudarsan, R.K. Vatsa, A.K. Tyagi, J. *Luminescence.,* 2009, **129**, 69–72.

18. Hongling Shi, Chen Zhu, Jiquan Huang, Jian Chen, Dongchuan Chen, Wenchao Wang, Fangyu Wang, Yongge Cao, and Xuanyi Yuan, *Optical Materials Express.,* 2014, **4**, 649.

19. Chung-Hsin Lu, and R. Jagannathan, *Appl. Phys. Letts.,* 2002*,* **80,** 3608.

20. K. Jayanthi, Santa Chawla, K.N. Sood, Manisha Chhibara, Sukvir Singh, *Appl. Surf. Sci*., 2009, 255, 5869–5875.

21. Hyun Kyoung Yang, and Jung Hyun Jeong, *J. Phys. Chem. C.,* 2010, **114***,* 226–230.

22. K. C. Misra, J. K. Berkowitz, K. H. Johnson, P. C. Schmidt, *Phys. Rev B.,* 1992, **45,** 10902.

23. J. C. Park, H. K. Moon, D. K. Kim, S. H. Byeon, B. C. Kim, K. S. Suh, *Appl. Phys. Lett.,* 2000, **77,** 2162.

24. May Nyman, Lauren E. Shea-Rohwer, James E. Martin, and Paula Provencio, *Chem. Mater.* 2009**, 21,** 1536–1542.

25. Jae-Wook Lee, Jae-Hyuk Lee, Eun-Ji Woo, Hyungwoong Ahn, Joon-Soo Kim, and Chang-Ha Lee, *Ind. Eng. Chem. Res.,* 2008, **47,** 5994–6000.

26. D. T. Mackay, C. R. Varney, J. Buscher, and F. A. Selim, *J. Appl. Phys.,* 2012, **112***,* 023522.

27. C. R. Varney, S. M. Reda, D. T. Mackay, M. C. Rowe, and F. A. Selim, *AIP Advances.,* 2011, **1,** 042170.

28. F. A. Selim, C. R. Varney, M. C. Tarun, M. C. Rowe, G. S. Collins and M. D. McCluskey, *Phys. Rev. B.,* 2013**, 88***,* 174102.

29. Ryo Kasuya, Tetsuhiko Isobe, Hitoshi Kuma, Junichi Katano, *J. Phys. Chem. B.,* 2005, **109,** 22126-22130.

30. M. E. Smith, G. Neal, M. B. Trigg, J. Drennan, *Appl. Magn. Reson*., 1993, **4,** 157-170.

31. W. S. Jung, S-K. Ahn. and Kim D-C, *J. Mater. Chem.,* 1998**, 8,** 1869.

32. G. Engelhardt, and D. Michel*, "High Resolution Solidstate Nmr Of Silicates And Zeolites" (John Wiley & Sons, Chichest*er, **1987**) P. 143.

33. K. J. D. Mackenzie, And T. Kemmitt, *Thermochim. Acta.,* 1999, **325***,* 13.

34. Potdevin A, Chadeyron G, Boyer D, Mahiou R, *J Mater Sci.,* 2006, **41***,* 2201–2209.

35. E. De La Rosa, L.A. Dı´Az-Torres, P. Salas, A. Arredondo. J.A. Montoya, C. Angeles, R.A. Rodrı´Guez,. *Opt. Mater.,* 2005, **27,** 1793–1799.

36. Ji Rongjin**,** Yin Wenhui**,** Fang Caixiang**,** and Zeng Yanwei**,** *J. Mater. Chem. C*., 2013, **1***,* 1763–1770.

37. Rebecca J. Holmberg, Tomoko Aharen, and Muralee Murugesu, *J. Phys. Chem. Lett.,* 2012**, 3,** 3721−3733.

38. Yao-Ming Hao, Shi-Yun Lou, Shao-Min Zhou, Rui-Jian Yuan, Gong-Yu Zhu, and Ning Li, *Nanoscale Research Letters.,* 2012**, 7,** 100.

39. Yüksel Köseo˘Glu, Hayrettin Yıldız, and Resul Yilgin, *Journal of Nanoscience and Nanotechnology.,* 2012, **12***,* 2261–2269.

40. Ilsu Rhee. *Journal of the Korean Physical Society.*, 2009, **54 (4),** 1721-1724.

41. Jiu-Ping Fan, Xiao-Li Li, Zhi-Yong Quan, and Xiao-Hong Xu, *Appl. Phys. Lett.,* 2013, **102,** 102407.

42. W. Q Zou, C. N. Ge, G. Venkataiah, H. L. Su, H. S. Hsu, J. C. A. Huang, X. C. Liu, F. M. Zhang, and Y. W. Du, *J. Appl. Phys.,* 2012, **111,** 113704.

43. R. M. Kadam, M. K. Bhide, M. D. Sastry, J. V. Yakhmi and O. Kahn, *Chemistry Physics Letters.,* 2002**, 357***,* 457-463.

44. D. Karmakar, S. K. Mandal, R. M. Kadam, P. L. Paulose, A. K. Rajarajan, T. K. Nath, A. K. Das, I. Dasgupta and G. P. Das, *Physical Review B.,* 2007, **75**, 144404.

45. S. V. Chong, K. Kadowaki, J. Xia, and H. Idriss, *Appl. Phys. Lett.* 2008, **92,** 232502.

46. X. W. Wang, X. P. Gao, G. R. Li, L. Gao, and T. Y. Yan, *Appl. Phys. Lett.*, 2007, **91***,* 143102.

47. Nadia Febiana Djaja, Rosari Saleh, *Materials Sciences and Applications.,* 2012**, 3,** 245-252.

48. R. V. Sagar, and S. Buddhudu, 2010, **75,** 1218- 1222.

49. S. Colis, A. Bouaine, G. Schmerber, C. Ulhaq-Bouillet, A. Dinia, S. Choua and P. Turek, *Phys. Chem. Chem. Phys.*, 2012, **14,** 7256–7263.

50. Xiaoyong Xu**,** Chunxiang Xu**,** Jun Da, Jingguo Hu**,** Fengji L**,** and Sam Zhang**,** ***J. Phys. Chem. C.***, 2012, **116,** 8813−8818.

51. Nguyen Hoa Hong, Joe Sakai, Nathalie Poirot, Virginie Brizé, *Phys. Rev. B***.,** 2006, **73,** 132404.

52. Monnier R, and Delley B, *Phys. Rev. Lett.,* 2001, **87**, 157204.

53. I. S. Elfimov, S. Yunoki, and G. A. Sawatzky, *Phys. Rev. Lett.,* 2002, **89,** 216403.

54. A. Zywietz, J. Furthmuller, and F. Bechstedt, *Phys. Rev. B.,* 2000, **62,** 6854.

55. S. Tsunekawa, K. Ishikawa, Z.Q. Li, Y. Kawazoe and A. Kasuya, *Phys. Rev. Lett.,* 2000, **85,** 3440.

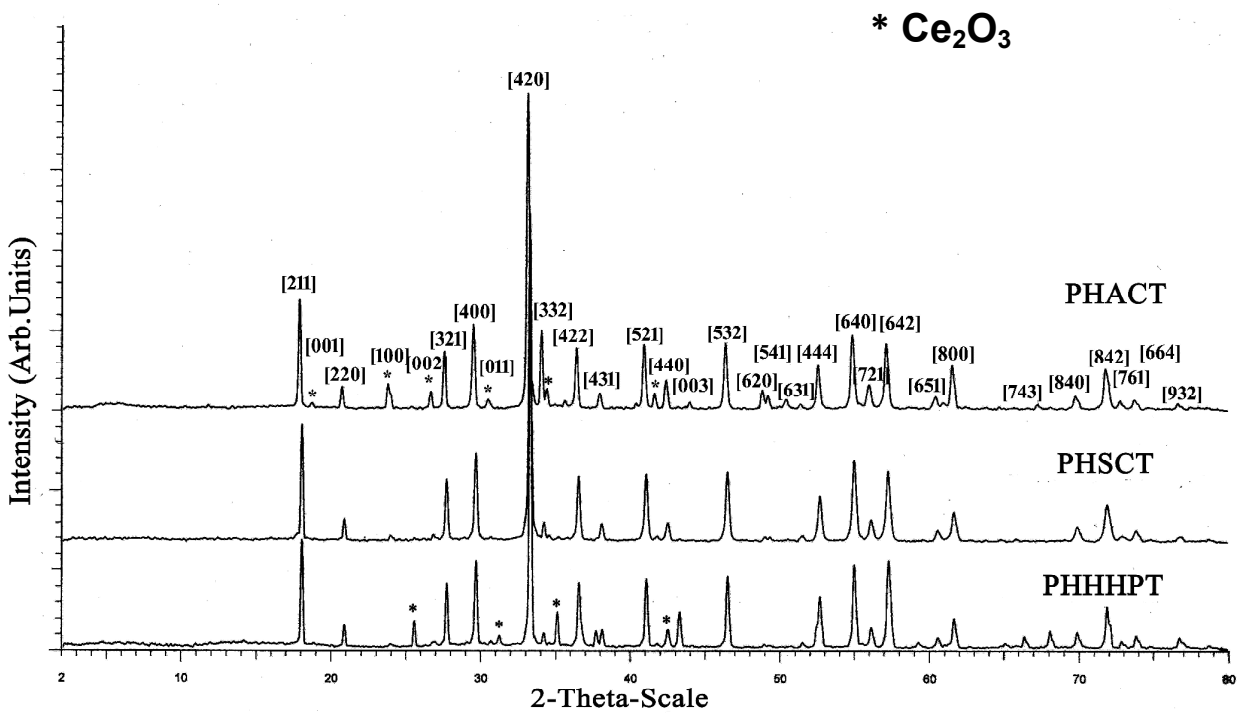

Figure 1. Structural properties of YAG:Ce NPs. An XRD pattern of the Ce doped YAG (0.1M) prepared under various synthesis methods shows purity and crystalline nature of the samples.

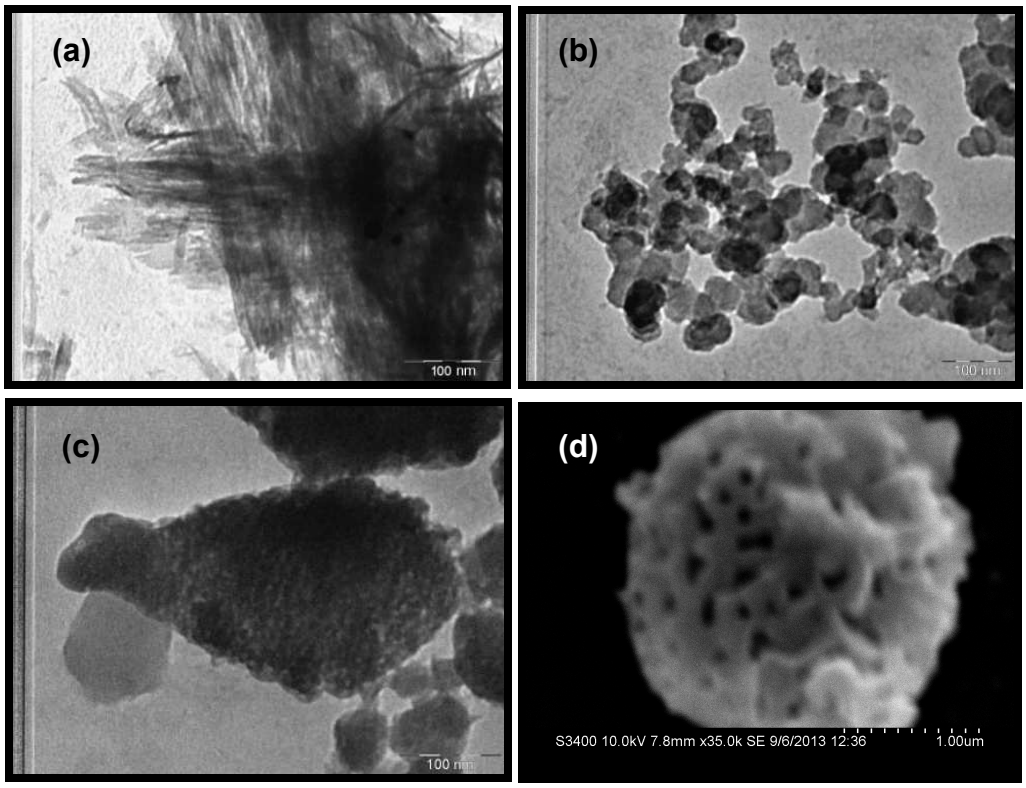

Figure 2. M**orphology of the YAG:Ce NPs.** TEM images of YAG:Ce NPs prepared by PHHHPT (b) PHACT (c) PHSCT. SEM images of NPs prepared by PHSCT is shown in Figure d

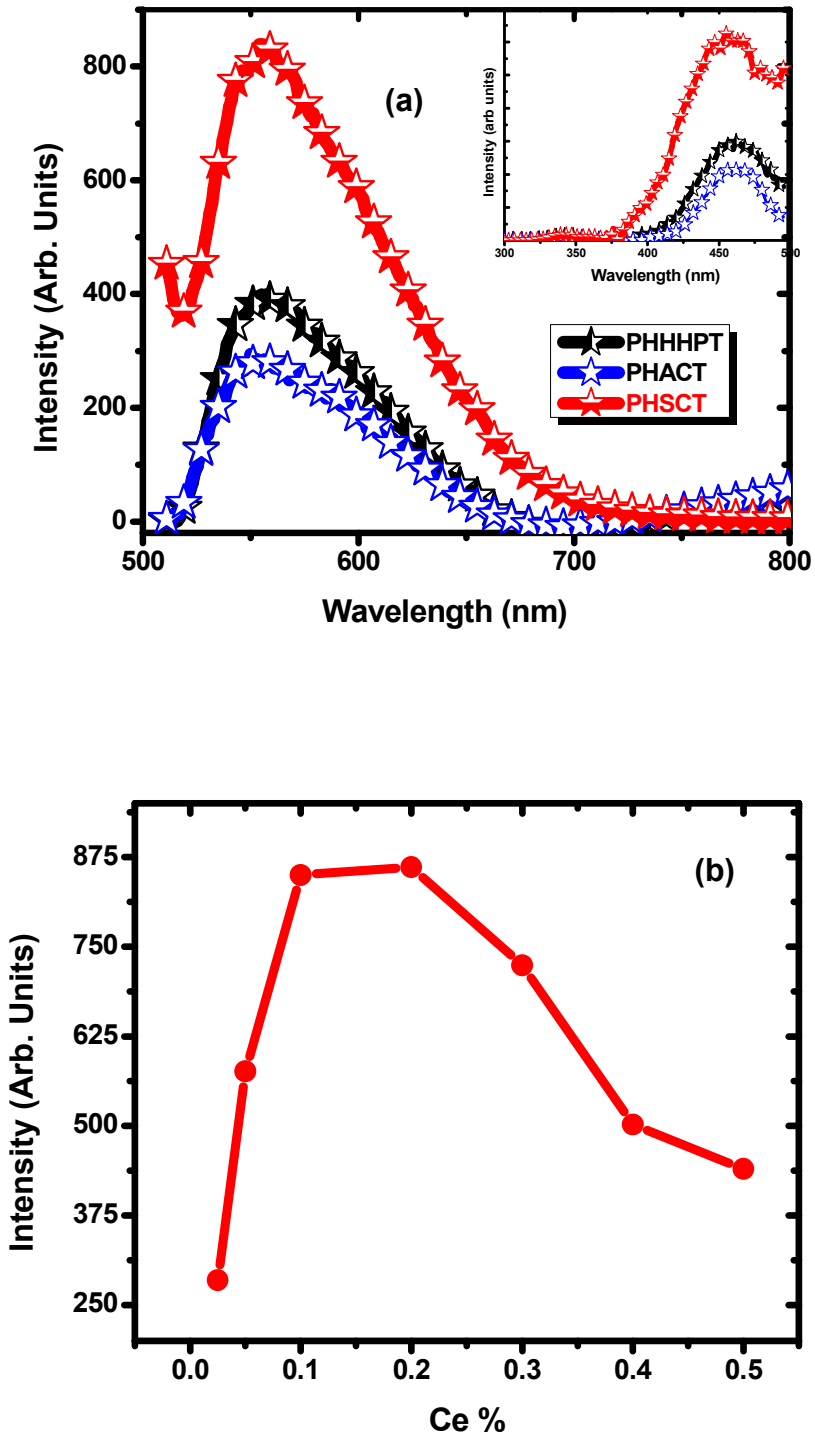

Fig 3. (Colour online) **Spectroscopic investigation of the YAG:Ce NPs**. (a) PL studies of the YAG:Ce NPs prepared by various synthesis techniques, (b)Variation in the PL intensity of YAG:Ce NPs prepared by PHSCT.

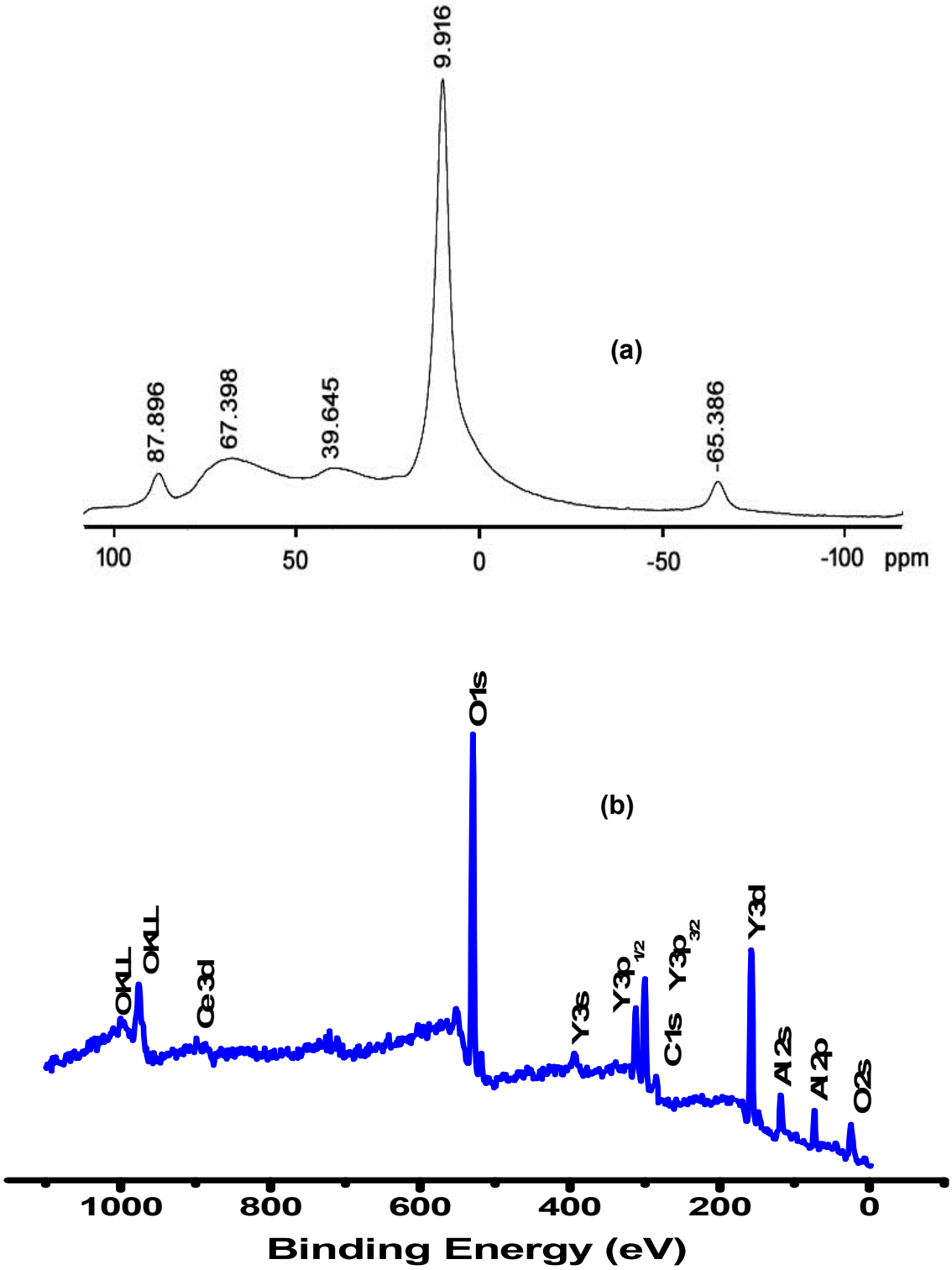

Fig 4. (Colour online) **Phase investigation of the YAG:Ce NPs**. (a) ^{27}Al solid state MAS-NMR studies of the YAG:Ce NPs prepared by PHSC technique, (b) XPS analysis of YAG:Ce NPs prepared by PHSCT.

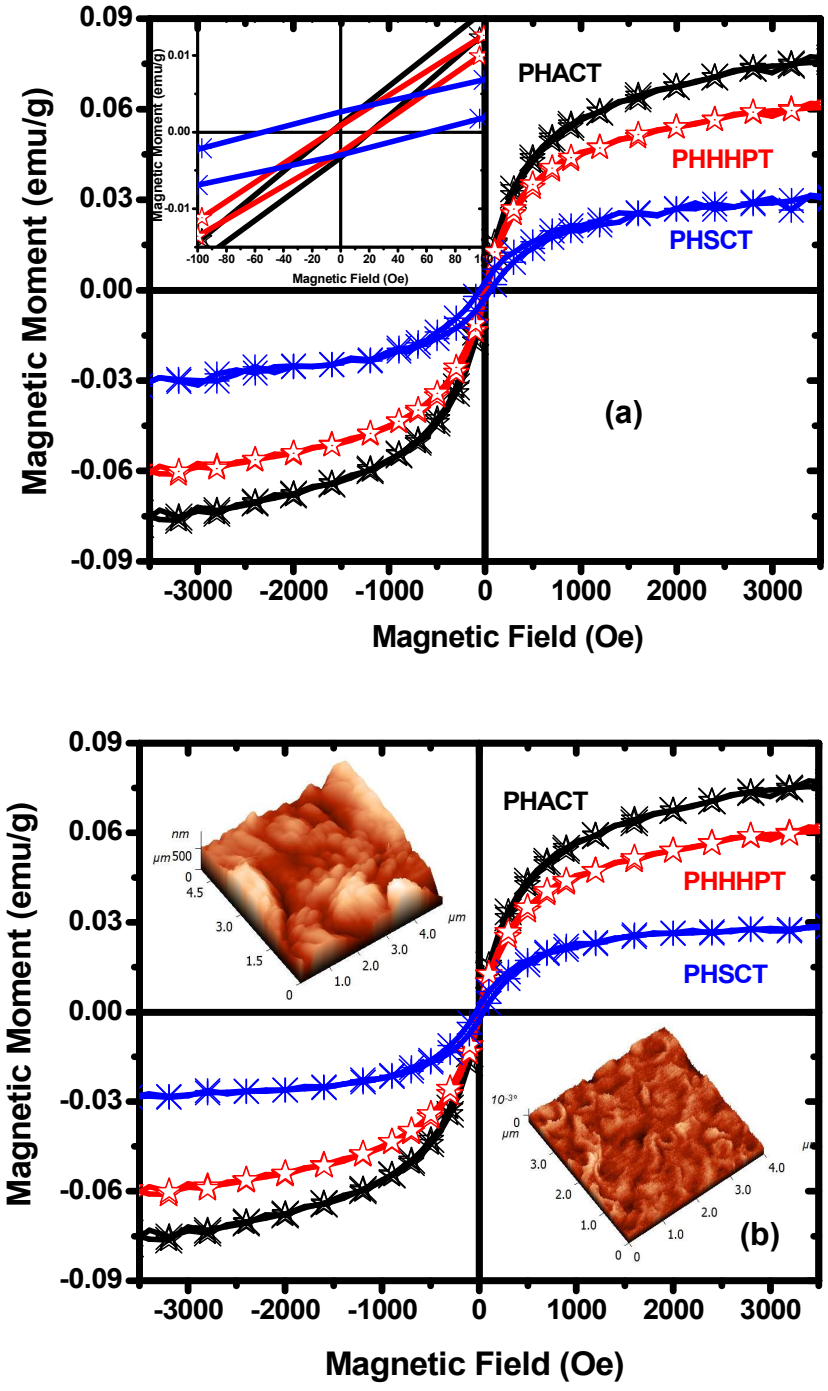

Figure 5. (Colour online) **Magnetic properties of undoped and Ce doped YAG NPs.** RT VSM plots of undoped (a) and Ce doped YAG (b) prepared under various synthesis condition shows similar Hysteresis loops behavior. The inset of Figure 5a shows magnified view of corresponding undoped YAG NPs to show coercive field and Figure 5b shows the AFM and MFM images of corresponding NPs

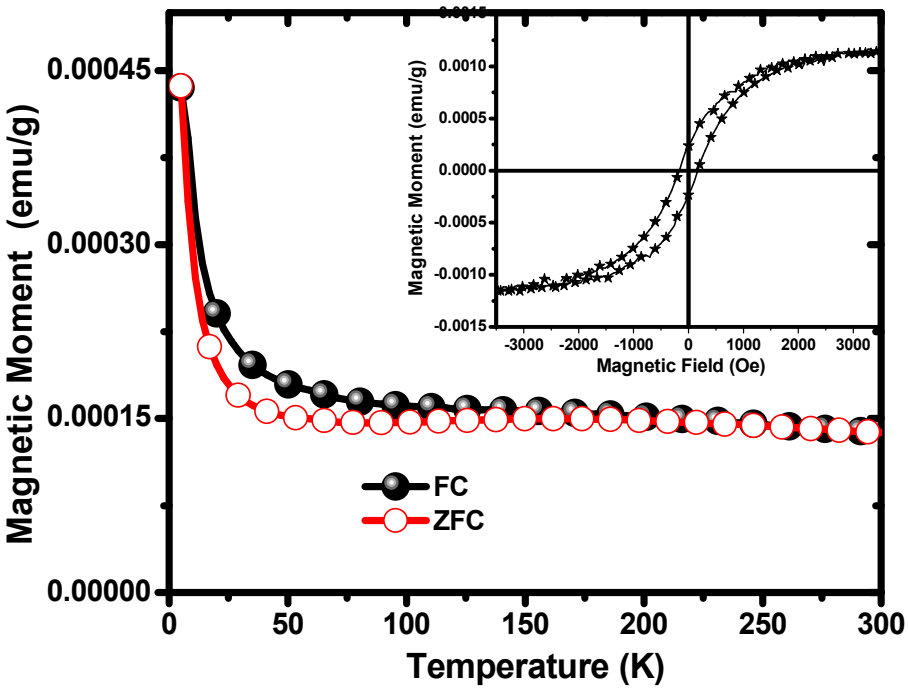

Figure 6. (Colour online) **Temperature dependence of the magnetization for YAG:Ce NPs**. Zero-field-cooled and field-cooled magnetization (applied field 100 Oe). The inset shows the hysteresis loops at RT for the same NPs.

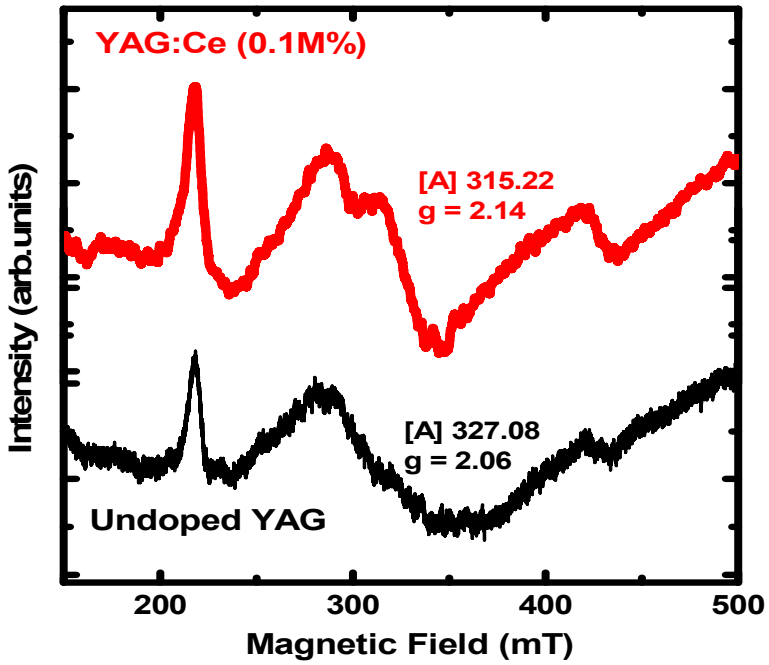

Figure 7. (Colour online) **ESR spectra of undoped and Ce doped (0.1M %) YAG NPs.** Origin of the ferromagnetism [oxygen vacancy] has been confirmed through EPR taken at RT.

Table 1

Crystalline parameters of undoped and Ce doped YAG NPs prepared by PHSC technique

Sample Details		**2Ɵ Values**	**Cell parameter (Å)**
Undoped YAG		33.289	12.0328
Ce Concentration	0.025M	33.257	12.0380
	0.05M	33.248	12.0411
	0.1M	33.191	12.0613
	0.2M	33.187	12.0618
	0.5M	33.212	12.0541

Table 2

RT Hc & M values of undoped and 0.1M% Ce doped YAG NPs

Sample Details	**PHSCT**		**PHHHPT**		**PHACT**	
	H_C (Oe)	**M memu/g**	**H_C (Oe)**	**M memu/g**	**H_C (Oe)**	**M memu/g**
YAG	54.50	31.83	17.54	62.27	17.29	78.14
YAG:Ce	41.14	28.79	14.77	61.81	14.23	77.23

- ***TABLE OF CONTENT***

Multifunctional lumino –magnetic YAG:Ce nanophosphors for LEDs and spintonics devices